ES Materials & Manufacturing

RESEARCH PAPER View Article Online

Possible Evidence of a Point of Discontinuity (T*) on the Arrhenius Relationship for the $Ba_{0.5}Sr_{0.5}Co_{1-x}Fe_xO_{3-\delta}$ Solid Solutions: A Non-Conventional Analysis

Edoardo Magnone,[1*] Grazia Accardo[2*] and Paolo Mele[3]

$Ba_{0.5}Sr_{0.5}Co_{1-x}Fe_xO_{3-\delta}$ solid solutions (x = 0.2, 0.5 and 0.8) have been studied by means of electrochemical impedance spectroscopy (EIS) in the temperature range of 500-800 °C under different atmospheres (oxygen and air). EIS measurements of oxygen reduction reaction (ORR) show a possible non-Arrhenius behavior at T*=680 °C. Moreover, this paper reviews the experimental evidence of a non-Arrhenius behavior (curvature) instead of a linear extrapolation commonly used in literature. Non-Arrhenius behavior is ascribed to a chemical step (Warburg-type impedance element) at a low-frequency range when the temperature is below T*. An electrochemical model is also tentatively proposed to explain the non-Arrhenius behavior of $Ba_{0.5}Sr_{0.5}Co_{1-x}Fe_xO_{3-\delta}$ at T*=680 °C.

Keywords: $Ba_{0.5}Sr_{0.5}Co_{1-x}Fe_xO_{3-\delta}$; Electrochemical Impedance Spectroscopy; Non-Arrhenius Behavior

Received 9 November 2018, **Accepted** 10 December 2018

DOI: 10.30919/esmm5f176

1. Introduction

Mixed ionic/electronic conducting (MIEC) ceramics have been studied and applied with success to solid oxide fuel cells (SOFC). In particular, the $Ba_{0.5}Sr_{0.5}Co_{1-x}Fe_xO_{3-\delta}$ (BSCF) electrode shows better electrocatalytic activity for oxygen reduction reaction (ORR) as compared with other perovskite-type electrodes[1] in the intermediate-temperature (IT) range between 500 and 800 °C.[2,3] The high electrochemical performance of BSCF probably is ascribed not only to its high oxygen vacancy concentration, which increases the oxygen bulk diffusion rate.[4] but also to extremely low electrochemical surface-related exchange resistance.[5]

A detailed description of the different controversial unsolved problems in the field of SOFCs cathode reaction process models is already reported in the previous literature.[2,4,6] The final understanding of nature and the role of MIEC cathode as $Ba_{0.5}Sr_{0.5}Co_{1-x}Fe_xO_{3-\delta}$ in SOFC is still under investigation.[7-18] In this connection, the reaction system in an SOFC (cathode/electrolyte/anode stack and its interconnects) is a very complex issue where, to complicate matters even further, different double- and triple-phase boundaries at the gas-electrode-electrolyte interfaces play important roles in the overall process.[1,2,4,13,19]

In this field, the electrochemical impedance spectroscopy (EIS) is an important tool of analysis to describe, to explain and to understand the electrochemistry-related problems[20,21] and, in particular, it is extensively used in the study of SOFC coupled with the determination of the "electrochemical activation energy" (E) regarding the electrode reactions. Generally, E was evaluated directly from the electrode resistance plots by a geometry-based equation of "Area Specific Resistance" (ASR) calculated, in turn, as:

$$ASR = R_p \frac{S}{2} \quad (1)$$

where R_p is the total interfacial polarization resistance obtained from impedance spectroscopy data in the complex impedance plane plots, and S is the apparent contact surface area in a symmetric two-electrode configuration. The value of S was calculated from geometrical factors unless otherwise specified. In a close temperature range, if the electrochemical system can be described by a single-activation-energy-controlled process, graphical methods can be used to obtain some electrochemical information. Arrhenius behavior, even for time-invariant electrochemical systems, is usually calculated with equation expressed as:

$$\mathbb{K} = A_0 e^{\left(-\frac{E}{RT}\right)} \quad (2)$$

where $\mathbb{K}$ is typically related to the rate of change of a resistance (i.e., ASR, circuit resistance, etc.) thermally activated; A_0 a pre-exponential term that, with the exception of few cases[22,23,24] often is not depth discussed in the literature; the (-E/RT) exponential expression describes the probability for the reaction to occur; E the average activation energy representing the thermal activation process in the temperature range studied where, intuitively, as the E increases, the catalytic reaction becomes less probable; R the universal gas constant; T the absolute temperature in Kelvin. All these variables differ quite a lot in the literature among different research works. Generally, the activation energy related to a simple thermally activated cathode can be derived

[1]*Department of Chemistry & Biochemical Engineering, Dongguk University, Manhae gwan - 30, Pildong-ro 1gil, Jung-gu, 100-715 Seoul, Republic of Korea*

[2]*Fuel Cell Research Center, Korea Institute of Science and Technology (KIST), Hwarangno 14-gil 5, Seongbuk-gu, 02792 Seoul, Republic of Korea*

[2]*SIT Research Laboratories, Shibaura Institute of Technology, 3-7-5 Toyosu, Koto-ku, 135-8548 Tokyo, Japan*

***E-mail:** magnone.edoardo@gmail.com*

from the slope of the corresponding Arrhenius plot in which K is plotted in a logarithmic scale against the reciprocal temperature (1/T).

This is not a trivial mathematical problem but may arise through the widespread use of Arrhenius-type equations.[25,26] In fact, the analysis is always based on the use of the Arrhenius equation and then it depends on the hypothesis that (1) a single reaction kinetic is set up through all double- and triple-phase boundary reaction zones, and (2) the chemical, physical and mechanical properties of the different phases are always constant and stable in the temperature or time range considered. In addition, various other assumptions are also necessary: (3) there is no significant overlap regarding the competitive/consecutive reactions in the studied system, and (4) the influence of electrical conductivity, crystalline defects, interdiffusion between phases, oxygen content (δ), phase transitions and/or stabilities, segregation of second phase particles, carbonation, etc. can be considered as marginal and does not have any influence on ASR.

All above suppositions are always implicitly assumed in a context where the temperature function is expressed only by a simple Arrhenius relationship.[7-15,19,23,24] In addition to all these hypotheses that should be confirmed by experimental evidence, there is also a conceptual problem of how to interpret the meaning of E[27-29] obtained by a single-step approximation (single Arrhenius equation) of, in reality, a multiple-step process.[30-32]

Among others, in the work of Chen *et al.* - in which EIS measurements were performed in order to measure the influence of Fe content (x) in $Ba_{0.5}Sr_{0.5}Co_{1-x}Fe_xO_{3-\delta}$ oxides on the electrode performance - is offer a clear example of a multiple step process studied and approximately described by a single-step approximation (single E)[12].

From Fig. 1a it can be noted that the high-temperature behavior is not consistent with this approximation because when the temperature increases (in particular above 700 °C), the ASR decreases sharply. With increasing temperature, as ASR increases, the experimental points reported by Chen *et al*. start to fall the predicted values according to a single Arrhenius interpretation.[12] As can be seen in Fig. 1a, a single extrapolation model cannot predict adequately the observed experimental data.[12] By contrast, Arrhenius plots of the experimental data reported by Chen *et al*. appear to consist with at least two activation energies at low and high temperature,[12] respectively, like many other interesting examples that can be found across the literature.[17,18] For example, it is evident in Fig. 1b that there is a discontinuity at about T*=680 °C between high (700 °C<T<800 °C) and low temperature (600 °C<T<650 °C) on the temperature dependence of the cathode polarization resistance (Rp) regarding the $Ba_{0.5}Sr_{0.5}Co_{0.2}Fe_{0.8}O_{3-\delta}$ sample.[17] In this particular case, it can be noted that the experimental points at low temperature (T=650, and 600 °C) are scattered loosely about a straight line according to a different angle of inclination than the above 700 °C (see Fig. 1b after Shen and Lu[17]). We faced the same situation not only for pure $Ba_{0.5}Sr_{0.5}Co_{0.8}Fe_{0.2}O_{3-\delta}$ cathode[17] but also for $Ba_{0.5}Sr_{0.5}Co_{0.8}Fe_{0.2}O_{3-\delta}$–$Sm_{0.5}Sr_{0.5}CoO_{3-\delta}$ composite cathode materials[18] where the point of discontinuity is again around T*=680 °C (Fig. 1b)

The Arrhenius-type distortion in the experimental EIS works for $Ba_{0.5}Sr_{0.5}Co_{1-x}Fe_xO_{3-\delta}$ solution series should be carefully monitored and treated, from both a practical and fundamental perspective. This investigation expands the experimental findings that have previously been published without any notice regarding the possible point of discontinuity around T*=680 °C. In this paper, the non-Arrhenius behavior in the $Ba_{0.5}Sr_{0.5}Co_{1-x}Fe_xO_{3-\delta}$ electrode on the temperature range of interest (500-800 °C) is studied and tentatively explained by a model derived from EIS measurements.

2. Experimental section

2.1 Sample preparation and characterization

The $Ba_{0.5}Sr_{0.5}Co_{1-x}Fe_xO_{3-\delta}$ solid solutions, with x = 0.2, 0.5 and 0.8, were prepared by the wet chemical procedure using stoichiometric amounts of nitrates as precursors and citric acid and ethylenediaminetetra acetic acid as complexing agents.[33] Barium (II) nitrate (99+%; Aldrich), strontium (II) nitrate (99+%; Aldrich), cobalt (II) nitrate hexahydrate (98+%, Aldrich), and iron (III) nitrate nonahydrate (98+%; Aldrich) were used as precursors. Other chemicals used for the synthesis are citric acid ($C_6H_8O_7 \cdot xH_2O$, Iso-for analysis, Carlo Erba reagents) and ethylenediaminetetraacetic acid ($C_{10}H_{16}N_2O_8$, EDTA, Iso-for analysis, Carlo Erba reagents). All reagents were used without further purification. The necessary amount of $Ba(NO_3)_2$ was first dissolved in an aqueous solution of EDTA–NH_3 (pH of about 6) under heating and

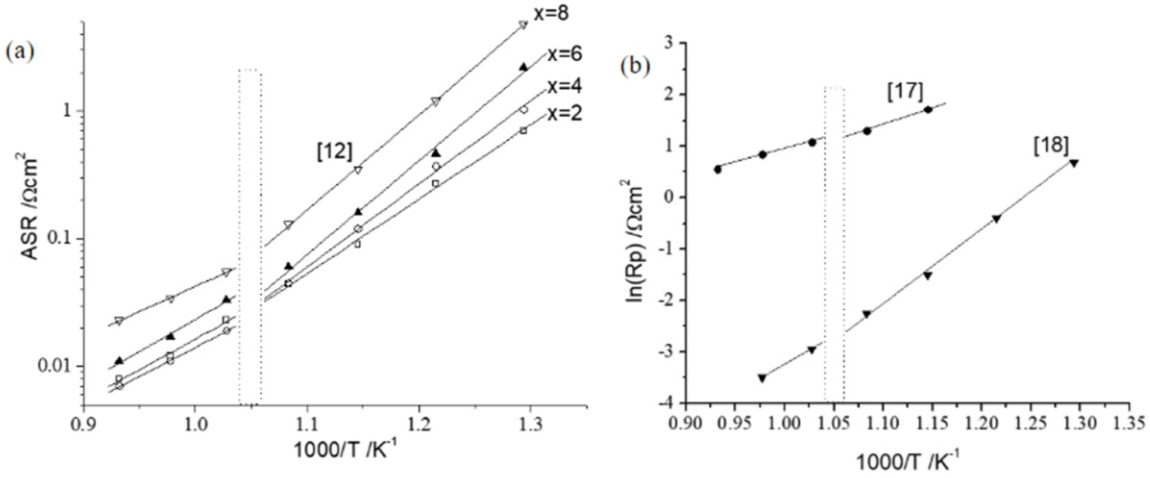

Fig. 1 Temperature dependence of the (a) Area Specific Resistance (ASR) for the $Ba_{0.5}Sr_{0.5}Co_{1-x}Fe_xO_{3-\delta}$ cathode with various Fe content (x) in a temperature range between 500 and 800 °C in the air after Chen *et al*.,[12] and the (b) polarization resistance (Rp) for the $Ba_{0.5}Sr_{0.5}Co_{0.2}Fe_{0.8}O_{3-\delta}$ (x=0.8) cathodes and $Ba_{0.5}Sr_{0.5}Co_{0.8}Fe_{0.2}O_{3-\delta}$–$Sm_{0.5}Sr_{0.5}CoO_{3-\delta}$ (x=0.2) composite cathode materials (70/30) after Shen and Lu[17] and Zhu *et al*.,[18] respectively. The points indicate the experimental data as reported in the previous works.[12,17,18] The solid line represents the curve of a probable evidence of a non-Arrhenius temperature dependence.

stirring, then the stoichiometric amounts of $Sr(NO_3)_2$, $Co(NO_3)_2$, and $Fe(NO_3)_3$ were added to the Ba-EDTA solution. After stirring, the proper amount of citric acid was introduced. The molar ratio of EDTA/citric acid/total metal ions was controlled to be 1:3:1. Upon evaporation of water, a dark purple transparent metal-organic gel was obtained, and then it was dried in a furnace overnight at 110 °C. The dried precursor gels were calcined for 2 h in synthetic air flux (30 mL/min) at 1100 °C with a heating rate of 7 °C/min and cooled at a rate of 3 °C/min. X-ray diffraction (XRD, Rigaku, Japan) was used to determine phase structures of the as-prepared $Ba_{0.5}Sr_{0.5}Co_{1-x}Fe_xO_{3-\delta}$ powders in the 2θ range of 20–80° with a step width of 0.02° at room temperature. XRD patterns of the samples were collected using $Cu_{K\alpha}$ radiation.

2.2 Electrochemical characterization

For electrochemical characterization, the $Ba_{0.5}Sr_{0.5}Co_{1-x}Fe_xO_{3-\delta}$ powders were deposited on SDC ceramic pellets. SDC powders (AGC Seimi Chemical Co., Ltd.) were uniaxially pressed into disks with a diameter of about 1 cm and thickness of about 0.3 cm and then sintered at 1600 °C for 10 h to obtain dense electrolyte pellets. Symmetrical $Ba_{0.5}Sr_{0.5}Co_{1-x}Fe_xO_{3-\delta}$/SDC/$Ba_{0.5}Sr_{0.5}Co_{1-x}Fe_xO_{3-\delta}$ cells were prepared by depositing the $Ba_{0.5}Sr_{0.5}Co_{1-x}Fe_xO_{3-\delta}$ electrodes on the SDC pellets. The calcined $Ba_{0.5}Sr_{0.5}Co_{1-x}Fe_xO_{3-\delta}$ electrode powders were mixed with the same volume of polyethyleneglycol and ethyl alcohol and then applied to the electrolyte by screen printing. The painted slurries were then fired at 1000 °C in the air for 1 h in order to minimize a possible interfacial reaction between the $Ba_{0.5}Sr_{0.5}Co_{1-x}Fe_xO_{3-\delta}$ cathode and SDC electrolyte.[34] The choice of relatively low firing temperature was found to be a good compromise in order to avoid a chemical interaction between electrodes and electrolyte and to have a sufficient interlayer adhesion strength between the components.[35]

EIS measurements were carried out under open circuit conditions by using a Solartron 1287 Potentiostat coupled with a 1260 Frequency Response Analyzer. The spectra were taken in the frequency range of 0.1 Hz to 5 kHz with a signal amplitude of 10 mV. The other details of the measurement and experimental condition are described in our previous report.[36]

3. Results and Discussion

3.1 Sample Characterization

Fig. 2 shows the XRD patterns of the $Ba_{0.5}Sr_{0.5}Co_{1-x}Fe_xO_{3-\delta}$ sample for Fe content (x=0.2) as a representative sample of the study. The diffraction patterns can be assigned to the single-cubic perovskite structure with space group *Pm3m* (JCPDS 055-0563) and no impurity phases were detected. Well-defined diffraction peaks are observed Fig. 2 and the peaks position in XRD pattern match well with other recent works.[37,38]

3.2 Electrochemical results (b)

From a qualitative point of view, all $Ba_{0.5}Sr_{0.5}Co_xFe_{1-x}O_{3-\delta}$ solid solution samples used in this study lead to very similar impedance spectra results across the three solid solutions (x = 0.2, 0.5 and 0.8). In the complex impedance plane, these are all characterized by different semicircles with a high-frequency intercept, as shown in Fig. 3a.

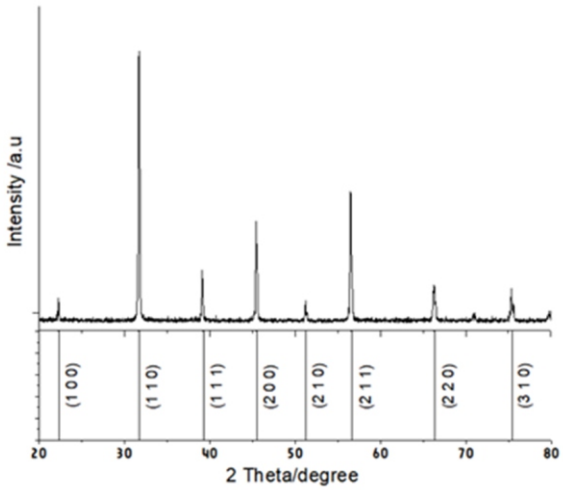

Fig. 2 Typical XRD pattern of $Ba_{0.5}Sr_{0.5}Co_{1-x}Fe_xO_{3-\delta}$ sample obtained by heating the x=0.2 composition powder precursor to 1100 °C for 2 h in synthetic air flux (30 mL/min). In the first approximation, the peaks can be indexed by a pseudocubic unit cell, as shown at the bottom of the pattern where the vertical tick marks indicate the position of allowed Bragg peaks in the *Pm3m* space group (JCPDS 055-0563). Data were collected at room temperature.

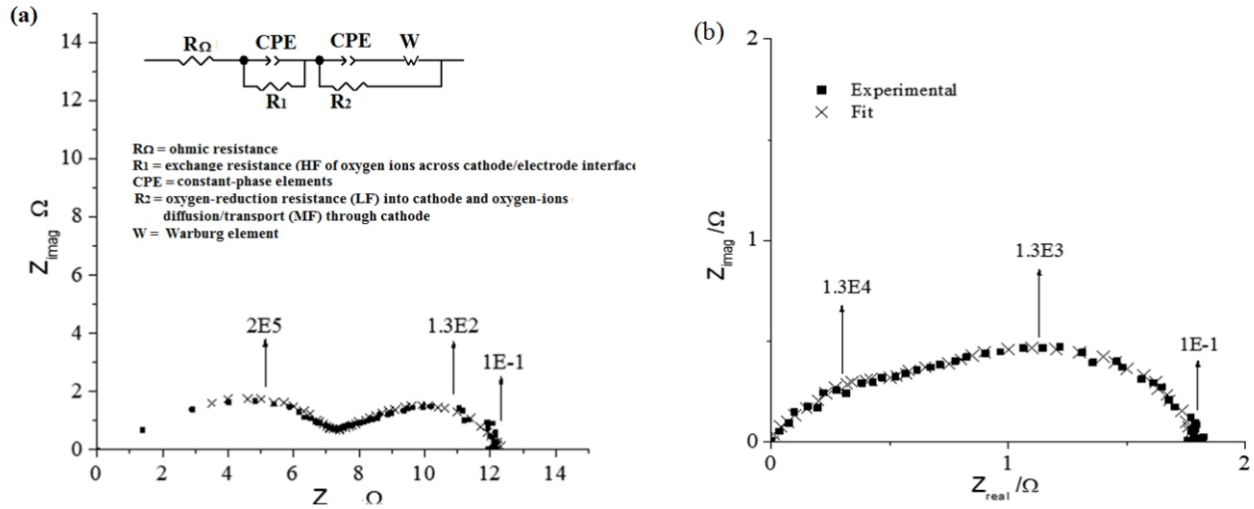

Fig. 3 Typical Nyquist plots of $Ba_{0.5}Sr_{0.5}Co_{1-x}Fe_{0.5}O_{3-\delta}$ electrodes (x=0.5) in symmetrical cells with SDC electrolyte in air at (a) 650 °C and (b) 700 °C. Inset: equivalent circuit representation of a process, where HF, MF, and LF denote the high, medium and low-frequency region, respectively, given in figure. The measured data (square) is shown together with the fitted data (cross).

The EIS experimental data have been fitted using an equivalent circuit (shown in the inset of Fig. 3a) similar to that already reported in literature.[5,11,39] The circuit consists of a series ohmic resistance, and two standard resistor-constant phase element (R-CPE) units. The simulation has led to the widespread use of a Warburg element in the equivalent circuit modelling. According to the data fitting, the intercept on the real axis at high frequency corresponds to the ohmic resistance (R), which includes the resistive contributions of the electrolyte, the electrode ohmic resistance and the lead resistance Across the arcs, the high-frequency resistance is associated with charge-transfer process (R_1) while the low-frequency arc (containing, in this case, the contribution at intermediate frequency) is ascribed to diffusion process (R_2), including adsorption-desorption of oxygen, oxygen diffusion at the gas-cathode interface, and the surface diffusion of intermediate oxygen species. The fit results show good agreement between the experimental and fitted data.

The Nyquist plot acquired at low-temperature range (Fig. 3a), for x=0.5, contain essentially three separable semicircle arcs arising from three relaxation processes of the electrode. The presences of three arcs indicate that at least three processes contributed to the oxygen reduction reaction (ORR). From a literature point of view, the semicircle at high frequency (HF) can be attributed to the processes occurring at the triple phase boundary (TPB) while the intermediate-frequency contribution (MF) can be correlated to the phenomenon occurring at regions within the electrode, farther away from the TPB. It is generally related to the dissociative adsorption of oxygen. The third response in the low frequency (LF) region depends on diffusion-adsorption of oxygen.

Focusing on the Nyquist diagram at 700 °C (Fig. 3b, the arcs are quite different from the plot acquired in the low-temperature range. In fact, two depressed arcs are visible and the plot consists of a much-depressed arc departing from the high-frequency range, which is well associated with both surface exchange and reduction resistance. The intermediate-frequency response is too weak in order to be detected and the lower frequency arc can be directly related to the TPB length and adjacent surface area of the phase facilitating dissociative adsorption. The amplitude of the arcs decreases with increasing the temperature and the contribution related to the diffusion process become predominant. In addition, the ohmic resistance, as well as the others resistances associated with the kinetics of electrode processes decrease with increasing temperature, as expected.

3.3 The Arrhenius behavior of the Area Specific Resistance (ASR)

The ASR variation with temperature for the studied $Ba_{0.5}Sr_{0.5}Co_{1-x}Fe_xO_{3-\delta}$ compositions (x = 0.2, 0.5 and 0.8) is shown in form of Arrhenius plots in Fig. 4. All samples show fully reversible conductivity behavior during the heating and cooling runs, and for clarity, only the data for the first cooling runs are here reported. The lowest values of ASR obtained were 0.56 Ωcm^2 for $Ba_{0.5}Sr_{0.5}Co_{0.2}Fe_{0.8}O_{3-\delta}$ in air and 0.25 Ωcm^2 for $Ba_{0.5}Sr_{0.5}Co_{0.8}Fe_{0.2}O_{3-\delta}$ in oxygen atmosphere at 800 °C. It should be noted that the temperature has almost no effect in a low-temperature range below T* of the Arrhenius plots, but has a significant effect at high temperature (700 > T > 800 °C). The Arrhenius plots for all compositions exhibit a linear behaviour in a low-temperature region up

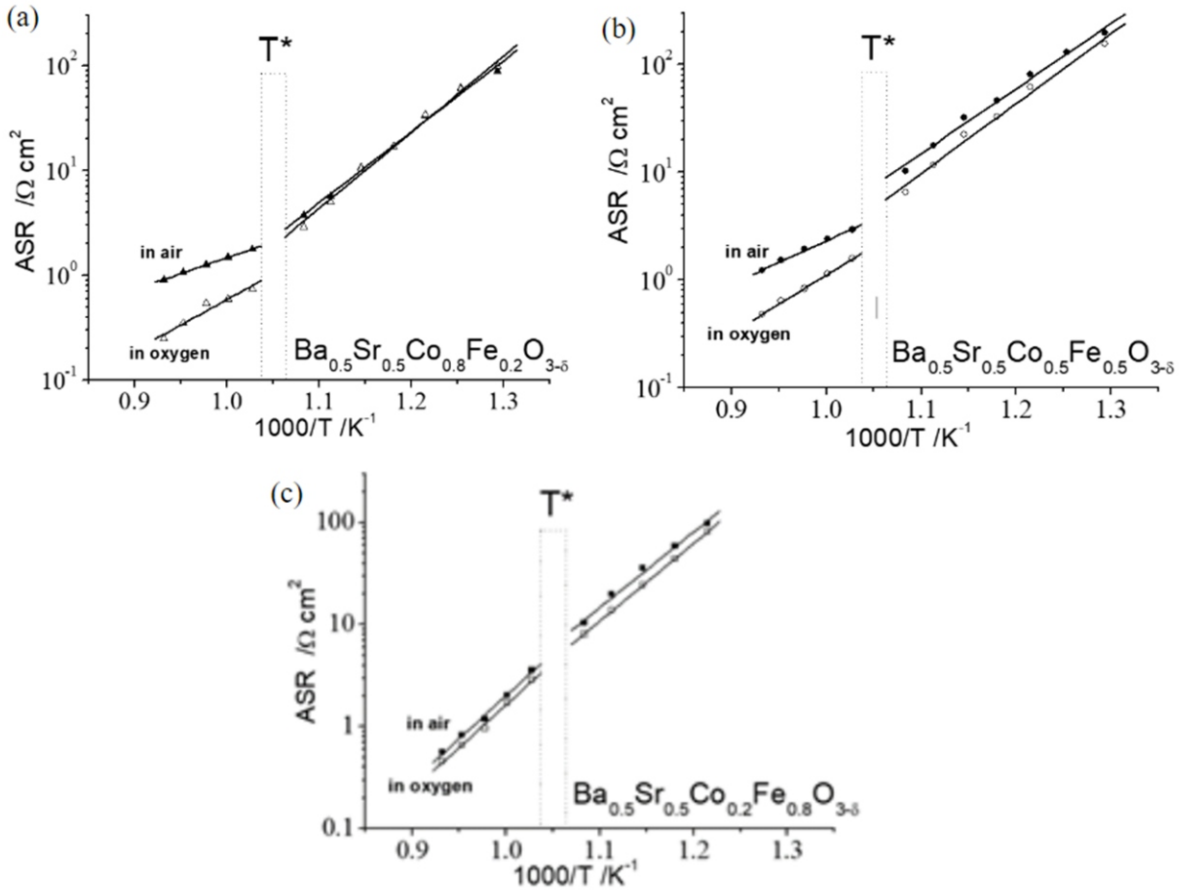

Fig. 4 Linear fit of the experimental points by two distinct Arrhenius laws below and above T*, respectively, of $Ba_{0.5}Sr_{0.5}Co_{1-x}Fe_xO_{3-\delta}$ electrodes with (a) x=0.2, (b) x=0.5 and (c) x=0.8, in a symmetrical cell with SDC as electrolyte, under different atmosphere (air and oxygen).

to around 700 °C. Between T* and 800 °C (see Fig. 4a, b and c) the plots show differing degrees of deviation from linearity and then a new linear region with different slope can be observed above T*.

A possible shift in the controlling kinetic processes provides a hypothesis that could explain the noticed phenomenon around T*. At a relatively low temperature between 500 °C and T* the slope is low in comparison with the high-temperature range above T* where the slope becomes greater. The ASR of all $Ba_{0.5}Sr_{0.5}Co_{1-x}Fe_xO_{3-\delta}$ samples, regardless of Fe content (x), increased with decreasing the temperature and, in addition, it shows little dependence on the oxygen partial pressure.

It is clearly shown that for all the samples, the curvature appears in the same temperature around T*. Moreover, it was also observed that the difference between ASR measured in air and oxygen atmospheres was larger with decreasing the Fe content (x).

As a consequence of the experimental evidence reported in Fig. 4, it can be hypothesized that there exists a kind of non-Arrhenius behavior (curvature) instead of the common single-step approximation[12,17,18] (see Fig. 1) in the Arrhenius plot regarding the $Ba_{0.5}Sr_{0.5}Co_xFe_{1-x}O_{3-\delta}$ solid solution with low and medium Fe content (x).

A great and fascinating variety of chemical and physical events occurs at the electrode/electrolyte interface and, among others, here we can cite the following: molecules adsorption, atoms, and molecules diffusion through the electrode/gas interface, surfaces reconstruction or ions rearrangement, electrons transfer between either the electrode and electroactive gas species, or to the various interfaces, and so on.[1,3] In addition to parameters like temperature and oxygen partial pressure, also the geometry and chemical composition of the TPB has a strong influence on the rate constant of the electrochemical reactions[2]. Some concurrent/consecutive processes that took place in the TPB can involve in more than only one type of energy barrier because the numbers and the natures of these transition-states change considerably during the course of measurements of electrochemical parameters in the whole temperature/time range investigated.

Under all these circumstances, it can be speculated from the above that also the Arrhenius parameters (i.e., A, Ea) are not constants with, for example, the temperature because there are linked with the relative chemical/physical variables of a given complex system. This could mean that if the carrier concentration is constant as a function of temperature, the Arrhenius plots of conductivity should be linear, where the pre-exponential constant A includes the carrier concentration as well as other material-dependent properties.[7-15,19,23-32] In most cases, if the charge carriers for a MIEC material are transported independently from each other, the total conductivity (σ_{tot}) can be written as the sum over the partial conductivities of all electronic (*el*) and ionic (*ion*) defects:

$$\sigma_{tot} = \sigma_{el} + \sigma_{ion} = \Sigma|Z_{i,el}|\, e\mu_{i,el}C_{i,el} + \Sigma|Z_{i,ion}|e\mu_{i,ion}C_{ion} \quad (3)$$

where, in general, the conductivity of particles "*i*" (σ_i) is proportional to the concentration (c_i) and the mobility (μ_i) of the carriers, as described by following equation:

$$\sigma_i = |Z_i|\, e\mu_i C_i \quad (4)$$

According to this principle, the contribution to the total conductivity brought by the first type of carriers is not influenced by the c_i and μ_i of the second, and vice versa. Thus, the Arrhenius plot is quite linear at a lower temperature with conductivity increasing as the temperature increases[40] because the ionic transport number in MIECs is still low and thus conductivities are represented by the σ_{el} contribution. However, it is well known that the carrier concentration of $Ba_{0.5}Sr_{0.5}Co_xFe_{1-x}O_{3-\delta}$ solid solution can be modified by the oxygen in the atmosphere at high temperature.[41] In fact, at higher temperatures, ionic compensation becomes significant as the oxygen content (δ) of the $Ba_{0.5}Sr_{0.5}Co_{1-x}Fe_xO_{3-\delta}$ electrodes decreases.[40] This means that a mechanism composed of single steps leads to a variety of complex transformations and transitions with the variation of temperature. In addition, it is also well known that usually the apparent diameter of the semi-circles merely corresponds to the interfacial polarization resistance (Rp) - which in first approximation includes the charge-transfer resistance of oxygen-ion transfer at electrode/electrolyte interface during electrochemical-kinetic steps (R2) - of chemical steps (Warburg-type impedance element, W) associated, in turn, with both chemical reactions at the electrode and the oxygen-ion diffusion resistance.

The defect chemistry of $Ba_{0.5}Sr_{0.5}Co_{1-x}Fe_xO_{3-\delta}$ solid solution system is extremely complex because both transition metal ions can adopt multiple valences depending on the oxygen content (δ) and then temperature and pressure.[1-3] On the basis of electrical conductivity data,[41,42] it is argued that the total electrical conductivity increases in air with increasing the temperature from room temperature to 400 °C, where it is dominated by p-type polaron hopping between $(Co^{3+}Co^{4+})_{1-x}(Fe^{3+}Fe^{4+})_x$ metal ions ratio, and then decreases between 400 and 1000°C not linearly but exponentially with different rates depending on the Fe content (x).[13,41] In addition, in the intermediate temperature domain the decrease in conductivity with increasing the temperature is most pronounced in $Ba_{0.5}Sr_{0.5}Co_{1-x}Fe_xO_{3-\delta}$ solid solutions having low Fe content (x=0.2) than high Fe content (x=0.8),[41] and a clear deviation from the linearity between the ln T and the 1/T is observed around 700 °C (with x=0.4, x=0.6, and x=0.8 in air[41] and with x=0.2 in N_2[43] as well as in other compositions[13]). The transition from localized to delocalized charge carriers was pointed out by others as well.[44,45] The temperature-dependent conductivity measurements show that there is an inversion in the trend of the total conductivity *versus* temperature between 680 °C and 550 °C for x=0.2 and x=0.8, respectively.[45]

3.4 Activation energies (Ea) versus Arrhenius relationship

With the aim of studying in depth the mechanisms involved in the responses of $Ba_{0.5}Sr_{0.5}Co_xFe_{1-x}O_{3-\delta}$ electrodes to the temperature (500-800 °C) and environmental factors, such as atmospheres (oxygen and air), it is necessary to control carefully the (1) Ea associated to the selected $Ba_{0.5}Sr_{0.5}Co_xFe_{1-x}O_{3-\delta}$ solid solutions, as well as all the (2) single circuit elements (R_1, R_2, and W) behavior in terms of T*. Consequently, the graphical results about Ea are shown in Figs. 4 (a, b, and c) and indicate simple linear regression through all experimental points for different temperature higher or lower than the T*. Notably, two Arrhenius relationships can perfectly simulate the experimental points below and above T*. As an indication, Table 1 gives the Ea values of three $Ba_{0.5}Sr_{0.5}Co_{1-x}Fe_xO_{3-}$ compositions (x=0.2, 0.5 and 0.8) not only calculated by a common single-step linear approximation (single Arrhenius equation[12,17,18]) in the whole IT range investigated (500-800 °C) but also by two non-Arrhenius-type behaviors that are distinguished in turn by different best-fit linear regression lines from 500 °C to T* and from T* to 800 °C, respectively. It can be noted that apparent Ea parameters, obtained by a single-step approximation are not in good agreement with each other for each compound, with the exception of $Ba_{0.5}Sr_{0.5}Co_{0.2}Fe_{0.8}O_{3-\delta}$ regardless of which atmosphere. In this last case with the x=0.8 composition in Fe the Ea calculated by a single Arrhenius law in the range 500-800 °C is quite similar to the energy values calculated by non-linear regressions using two Arrhenius equations above and below T*.

Clearly, Ea calculated by single-step approximation (Ea_{tot} in Table 1) in the overall range 500-800 °C increases substantially with increasing the Fe content (x) and, in more detail, we observe that the Ea_{tot} values for the x=0.2, x=0.5 and x=0.8 samples found to be 1.07, 1.51 and 1.70 eV, respectively. Conversely, if these data were treated as two different processes, the samples with a lower Fe content (x=0.2) possess very low Ea above T* (Ea=0.68 eV) than at low temperatures below T* (Ea=1.38) in the air as well as in oxygen. In contrast, $Ba_{0.5}Sr_{0.5}Co_{1-x}Fe_xO_{3-\delta}$ samples with high Fe content (x=0.8), the Ea associated to the high-temperature region (above T*) has higher values (Ea=1.77 eV) than at lower temperatures (Ea=1.54). It appears that the intermediate case, $Ba_{0.5}Sr_{0.5}Co_{1-x}Fe_xO_{3-\delta}$ samples with x=0.5 is a compromise between these two types of behaviors and it is strongly dependent on gas conditions. From this, it can be concluded that there is a kind of shift in the controlling mechanism around T*. As we noted above, a similar fall in the ASR has been reported indirectly by Chen *et al*. in his work on the influence of Fe content (x) in $Ba_{0.5}Sr_{0.5}Co_{1-x}Fe_xO_{3-\delta}$ oxides[12] as well as in other papers.[17,18]

3.5 The Arrhenius behavior of the equivalent circuit elements

In order to better understand the reaction mechanism and the actual evidence on discontinuities in the Arrhenius plots around T*, the R1, R2, and W1 elements (see Fig. 3) have also been calculated and represented as a function of reciprocal of temperature in Fig. 5a, b and

Table 1 Calculated activation energy (eV) of $Ba_{0.5}Sr_{0.5}Co_{1-x}Fe_xO_{3-\delta}$ solid solutions (x = 0.2, x=0.5, and 0.8) by the impedance study carried out in different atmospheres below and above T* as well as on the whole temperature range investigated.

x		Ea Below T*	R2	Ea Above T*	R2	Ea_{tot} (500-800 °C)	R^2_{tot}
0.2	air	1.38	0.9951	0.68	0.9994	1.07	0.9658
0.2	O_2	1.52	0.9913	1.05	0.9399	1.57	0.9737
0.5	Air	1.32	0.9919	1.98	0.9330	1.51	0.9611
0.5	O_2	1.36	0.9868	1.17	0.9997	1.67	0.9827
0.8	Air	1.54	0.9921	1.77	0.9941	1.70	0.9968
0.8	O_2	1.46	0.9958	1.74	0.9932	1.68	0.9988

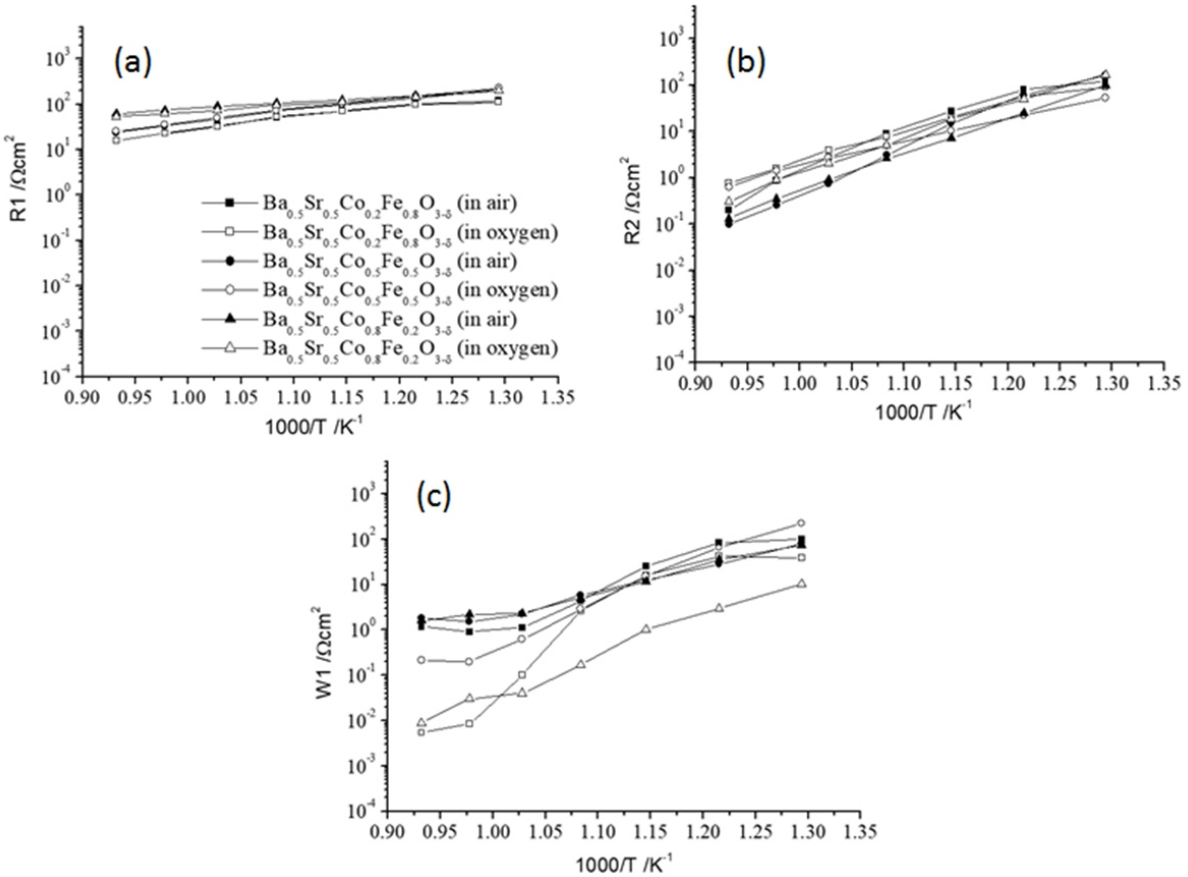

Fig. 5 Arrhenius plot of the equivalent circuit elements (R1, R2 and W1) calculated for the $Ba_{0.5}Sr_{0.5}Co_{1-x}Fe_xO_{3-\delta}$ electrodes (x=0.2, 0.5 and 0.8) under different atmospheres (air and oxygen). The solid lines serve as eye-guides and indicate the general trend of the temperature dependence.

c, respectively. It can be seen that R1 (Fig. 5a) - associated with charge-transfer process - increases slightly for all samples with increasing temperature in the overall range 500-800 °C without any apparent discontinuities at T* regardless of the atmosphere. The same behavior is observed in R2 values - resistance ascribed to diffusion process (i.e., adsorption-desorption of oxygen, oxygen diffusion at the gas-cathode interface, surface diffusion of intermediate oxygen species, etc) - regardless of the Fe content (x) and gas (Fig. 5b). On the other hand the W resistance (Warburg-type impedance element) follows a linear Arrhenius equation only at low temperature (below T*) and then the data are quite scattered at low values, but still suggest a monotonic relationship between the W and the inverse of temperature in the Arrhenius plot shown in Fig. 5b. Specifically, in the case of low (x=0.2) and medium (x=0.5) Fe contents in the temperature range between T* and 800°C when the samples were exposed to the oxygen, the plots show a significant negative deviation from Arrhenius linearity.

This study not only show these associations, but it can be speculated that the chemical steps associated with W (i.e., resistances of oxygen adsorption-reduction and oxygen-ion diffusion in the bulk) decreases with increasing the temperature more than R_1 and R_2 above T* so that on this temperature there is the appearance of a point of discontinuity on the Arrhenius relationship for the $Ba_{0.5}Sr_{0.5}Co_{1-x}Fe_xO_{3-\delta}$ solid solution series.

4. Conclusions

The analysis of the impedance diagrams revealed the presence of at least two or three processes involved in the ORR according to the operative temperature and the experimental gas conditions. The first process, occurring at high-frequency (HF), was assigned to interfacial electrochemical-kinetic processes (exchange of oxygen ions across the cathode/electrolyte interface). The second one, at the intermediate-frequency (MF), low frequency in the case of two processes was associated with dissociative adsorption process while the third contribution at the low-frequency (LF) was related to the chemical steps (resistances of oxygen-reduction and oxygen-ion diffusion through the bulk).

The hypothesis concerning a non-simple Arrhenius-type mechanism for $Ba_{0.5}Sr_{0.5}Co_xFe_{1-x}O_{3-\delta}$ solid solution system is confirmed from an electrochemical point of view by the agreement between the impedance element values (R1, R2, W1) as an function of the inverse of temperature in the Arrhenius plot calculated by EIS measurements and those obtained from a common single-step approximation (single Arrhenius equation). This paper constitutes not only a summary but also a critical evaluation of the present status of the Arrhenius law and its right application to the electrochemical study regarding the extremely complex solid solution systems like the selected $Ba_{0.5}Sr_{0.5}Co_xFe_{1-x}O_{3-\delta}$. Clearly, given these results, additional studies are required to further clarify the specific role of Fe content (x) as well as Co content (y) in determining the non-Arrhenius behavior for the $Ba_{1-y}Sr_yCo_{1-x}Fe_xO_{3-d}$ solid solutions.

Conflict of interest

There are no conflicts to declare.

References

1. Z. Shao and S. M. Haile, *Nature*, 2004, **431**, 170-173.
2. S. B. Adler, *Chem. Rev*., 2004, **104**, 4791-4844.
3. A. Tarancon, *Energies*, 2009, **2**, 1130-1150.
4. W. Zhou, R. Ran and Z. Shao, *J. Power Sources*, 2009, **192**, 231-246.
5. F. S. Baumann, J. Maier and J. Fleig, *Solid State Ionics*, 2008, **179**, 1198-1204.
6. Y. Li, R. Gemmen and X. Liu, *J. Power Sources*, 2010, **195**, 3345-3358.
7. S. Lee, Y. Lima, E. A. Lee, H. J. Hwang and J. W. Moon, *J. Power Sources*, 2006, **157**, 848-854.
8. Q. L. Liu, K. A. Khor and S. H. Chan, *J. Power Sources*, 2006, **161**, 123-128.
9. C. H. Chen, C. Li. Chang and B. H. Hwang, *Mater. Chem. Phys*., 2009, **115**, 478-482.
10. W. Zhou, R. Ran, Z. Shao, R. Cai, W. Jin, N. Xu and J. Ahn, *Electrochimica Acta*, 2008, **53**, 4370-4380.
11. F. S. Baumann, J. Fleig, H. U. Habermeier and J. Maier, *Solid State Ionics*, 2006, **177**, 3187-3191.
12. Z. Chen, R. Ran, W. Zhou, Z. Shao and S. Liu, *Electrochimica Acta*, 2007, **52**, 7343-7351.
13. X. Ding, X. Kong, J. Jiang, C. Cui and X. Guo, *Mater. Res. Bull.*, 2010, **45**, 1271-1277.
14. Y. Lin, R. Ran and Z.Shao, *Int. J. Hydrogen Energy*, 2010, **35**, 8281-8288.
15. Y. Lin, R. Ran, Y. Zheng, Z. Shao, W. Jin, N. Xu and J. Ahn, *J. Power Sources*, 2008, **180**, 15-22.
16. S. Suna and Z. Cheng, *J. Electrochem. Soc.*, 2017, **164**, F3104-F3113.
17. F. Shen and K. Lu, *Fuel Cell*, 2018, **18**, 457-465.
18. W. Zhu, Z. Lü, S. Li, B. Wei, J. Miao, X. Huang, K. Chen, N. Ai and W. Su, *J. Alloys Compd.*, 2008, **465**, 274-279.
19. Y. Fujimaki, K. Mizuno, Y. Kimura, T. Nakamura, K. Develos-Bagarinao, K. Yamaji, K. Yashiro, T. Kawada, F. Iguchi, H. Yugami and K. Amezawa, *ECS Trans*., 2017, **78**, 847-853.
20. B. Y. Chang and S. M. Park, *Annu. Rev. Anal. Chem.*, 2010, **3**, 207-229.
21. D. Macdonald, *Electrochimica Acta*, 2006, **51**, 1376-1388.
22. H. Paradis, M. Andersson, J. Yuan and B. Sundén, *J. Fuel Cell Sci. Technol*, 2011, **8**, 031014-031022.
23. E. Magnone, H. J. Lee and J. H. Park. *J. Chem. Eng. Commun.*, 2015, **202**, 1261-1270.
24. C. Bernuy-Lopez, L. Rioja-Monllor, T. Nakamura, S. Ricote, R. O'Hayre, K. Amezawa, M.-A. Einarsrud and T. Grande, *Materials*, 2018, **11**, 196-212.
25. J. H. Flynn, *Thermochimica Acta*, 1997, **300**, 83-92.
26. A. K. Galwey, *Thermochimica Acta*, 2003, **399**, 1-29.
27. A. K.Galwey, *Thermochimica Acta*, 2003, **397**, 249-268.
28. S. Vyazovkin, *Thermochimica Acta*, 2003, **397**, 269-271.
29. S. Vyazovkin, *Int. Rev. Phys. Chem.*, 2000, **19**, 45-60.
30. P. Simon, *J. Therm. Anal. Calorim.*, 2005, **79**, 703-708.
31. P. Simon *J. Therm. Anal. Calorim.*, 2005, **82**, 651.
32. P. Simon, *J. Therm. Anal. Calorim.*, 2007, **88**, 709.
33. E. Magnone, M. Miyayama and E. Traversa, *J. Electrochem. Soc.*, 2009, **156**, B1059-B1066.
34. B. Wei, Z. Lü, X. Huang, S. Li, G. Ai, Z. Liu and W. Su, *Materials Letters*, 2006, **60**, 3642-3646.
35. K. Wang, R. Ran, W. Zhou, H. Gu, Z. Shao and J. Ahn, *J. Power Sources*, 2008, **179**, 60-68.
36. E. Magnone, E. Traversa and M. Miyayama, *J. Electrochem. Soc.*, 2010, **157**, B357-B364.
37. S. Li, Z. Lü, X. Huang, B. Wei and W. Su, *J. Phys. Chem. Solids*, 2007, **68**, 1707-1712.
38. A. Fares, A. Barama, S. Barama, N. FodilCherif and M. L. Chelaghmia, *Electroanalysis*, 2017, **29,** 2323-2331.
39. P. R. Kautkar, S. C. Shirbhate and S. A. Acharya, *AIP Conference Proceedings*, 2018, 090057 doi:10.1063/1.5032904.
40. J. W. Stevenson, T. R Armstrong, R. D. Carneim, L. R. Pederson and L. Weber, *J. Electrochem. Soc.*, 1996, **143**, 2722-2729.
41. J. I. Jung, S. T. Misture and D. D. Edwards, *J. Electroceramics*, 2010, **24**, 261-269
42. J. Peña-Martínez, D. Marrero-López, J. C. Ruiz-Morales, P. Núñez, C. Sánchez-Bautista, A. J. Dos Santos-García and J. Canales-Vázquez, *Int. J. Hydrogen Energy*, 2009, **34**, 9486-9495.
43. M. Darab, M. S. Toprak, G. E. Syvertsen and M. Muhammed, *J. Electrochem. Soc.*, 2009, **156**, 139-143.
44. J. I. Jung, S. T. Misture and D. D. Edwards, *Solid State Ionics*, 2012, **206**, 50–56.
45. A. S. Harvey, F. J. Litterst, Z. Yang, J. L. M. Rupp, A. Infortuna and L.J. Gauckler, *Phys. Chem. Chem. Phys.*, 2009, **11**, 3090-3098.